Received 9 May 2021; revised 2 June 2021; accepted 7 June 2021. Date of publication 21 June 2021; date of current version 6 July 2021.

Digital Object Identifier 10.1109/OJAP.2021.3090908

A Millimeter-Wave Frequency Reconfigurable Circularly Polarized Antenna Array

MARIOS PATRIOTIS[1] (Student Member, IEEE), FIRAS N. AYOUB[1], YOUSSEF TAWK[2] (Senior Member, IEEE), JOSEPH COSTANTINE[2] (Senior Member, IEEE), AND CHRISTOS G. CHRISTODOULOU[1] (Life Fellow, IEEE)

[1]Electrical and Computer Engineering Department, University of New Mexico, Albuquerque, NM 87131, USA

[2]Electrical and Computer Engineering Department, American University of Beirut, Beirut 1107 2020, Lebanon

CORRESPONDING AUTHOR: Y. TAWK (e-mail: yatawk@ieee.org)

This work was supported by the Bluecom Systems and Consulting under Subcontract BC2016001 from the Phase II NASA STTR under Contract NNX17CC01C.

ABSTRACT This paper discusses the design of a high gain right-hand circularly polarized millimeter-wave frequency reconfigurable antenna array. The 16-element antenna array is designed to reconfigure its operating frequency over both K- and Ka-bands. More specifically, the reconfigurability is ensured through the integration of a modified ring resonator along with the array's sequentially rotated stacked feeding network. The ring resonator is designed to reconfigure its operating frequency over four distinct bands with center frequencies at 25 GHz, 26 GHz, 27.75 GHz and 29 GHz, respectively. Such integration enables the proposed millimeter-wave antenna array to exhibit unique radiation characteristics by maintaining circular polarization with an Axial Ratio (AR) $<$ 1 dB in a fractional bandwidth of 37.5% between 21.2 GHz and 31 GHz. A Figure of Merit that takes into account the array's axial ratio, sidelobe levels and fractional bandwidth is developed to highlight the unique performance of the presented millimeter-wave circularly polarized array in comparison to available work in the literature. The fabricated antenna array shows good agreement with the simulated data where it is found that the measured realized gain exceeds 12 dBic with sidelobe levels of less than -17.5 dB over the various frequency bands of the frequency reconfigurable antenna array.

INDEX TERMS Frequency reconfiguration, PIN diodes, filtenna, band pass filter.

I. INTRODUCTION

FREQUENCY reconfigurable circularly polarized antenna arrays are required for future millimeter-wave based communication systems. Frequency reconfiguration can be mainly achieved by manipulating the surface currents on the antenna [1]–[4] or by tuning the feeding network through the integration of a reconfigurable bandpass filter (BPF) [5], [6]. Such integration eliminates the incorporation of active components on the radiating surface and accordingly reduces the effects of the DC biasing network on the antenna radiation characteristics.

Several reconfigurable BPFs are introduced in the literature using cross-shaped and loop-shaped resonator structures [7]–[9]. These BPFs share the common principle of odd/even mode analysis and are designed to enable a change in their operation either from narrowband to wideband or from band-stop to band-pass. The enhancement in the filter's selectivity is achieved by implementing ring resonator designs with additional transmission zeros through the incorporation of stubs, inter-digital capacitors, filter cascading, or by adopting the transversal signal interaction principle [10]–[12].

The design of circularly polarized antenna structures is also widely covered in the literature [13]–[17]. One of the techniques relies on dual-band elliptically polarized curl patches that are aperture-fed using a substrate integrated waveguide (SIW) feeding network [13]. In [14] and [15], circular polarization is achieved by utilizing narrowband

circularly polarized truncated rectangular patches. The patches are orthogonally oriented with respect to each other and fed using a combination of a sequential rotation and a parallel feeding network to form a single layer *N*-element antenna array. In [16], a wideband linearly polarized element placed in a cross configuration is fed by a double sequential feeding network in order to excite circular polarization.

In this paper, a bandpass filter (BPF) composed of a modified ring resonator that is terminated by tunable loads for operation at both K- and Ka-bands is proposed. The change in the load impedance enables the filter to reconfigure its band-pass range. More specifically, the load impedances are formed by relying on shunt open stubs that can be dynamically extended using RF PIN diode switches (i.e., MA4AGP907). The BPF is designed to cover the span of frequencies between 23.75 GHz to 30.1 GHz, with four tunable bands. The proposed reconfigurable filter structure is then integrated into the double sequentially rotated feeding network of a broadband right hand circularly polarized 16-element patch array. Such integration enables the array to reconfigure its operating frequency while maintaining a circularly polarized behavior. A figure of merit is provided to highlight the novel features of the proposed millimeter-wave array in achieving high gain (>12 dBic), circularly polarized radiation with sidelobe levels less than −17.5 dB, and an axial ratio < 1 dB for a fractional bandwidth of 37.5% (i.e., 21.2 GHz – 31 GHz).

Section II of this paper details the design of the reconfigurable BPF. Section III describes the 16-element antenna array design along the integration of the filter within the antenna array feeding network for frequency reconfiguration. The measured assessment of the fabricated prototypes for both the antenna array and the frequency reconfigurable structure are presented in Section IV. Section V concludes the paper.

II. MODIFIED RING RESONATOR FILTER DESIGN

A ring resonator can be implemented as a band-pass filter when the two filter's RF ports are capacitively connected to the ring. The corresponding operating frequency of the filter is defined by the wavelength that matches the circumference of the ring. Thus, if the circumference is altered, a change in the filter's operating bandwidth is obtained. Such alteration can be achieved by terminating the ring with reactive loads in the form of open or short stub sections. The extension of the length of these stubs entails a change in the load impedance and accordingly a change in the filter's operating band-pass range. The change in the stub's reactive impedance is controlled by extending the stub's length through the activation of RF PIN diode switches.

The proposed filter topology that is designed on a 0.5 mm thick RO3003 substrate ($\varepsilon_r = 3$ and $\tan\delta = 0.0012$) is presented in Fig. 1 with total dimensions of (12 mm x 14 mm). A ring with a width of 0.1 mm is capacitively coupled to the two filter's ports through two 50 Ω, 1.3 mm

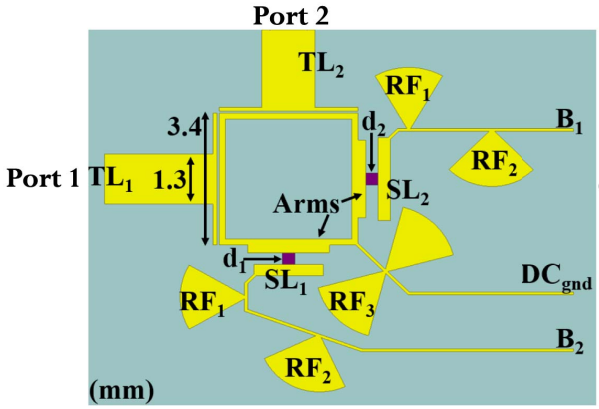

FIGURE 1. The proposed reconfigurable modified ring resonator BPF with the integrated two PIN diodes and the corresponding biasing network.

wide, transmission lines $\mathtt{TL}_1$ and $\mathtt{TL}_2$. Such capacitive coupling is implemented on two sides of the ring through a 0.05 mm gap. The other two sides of the ring are connected to 0.2 mm x 2 mm open loads labeled as Arms in Fig. 1. To achieve frequency reconfiguration, the lengths of these two open loads are extended by connecting two PIN diode switches d_1 and d_2 to two additional stubs SL_1 and SL_2. These two stubs share the same width of 0.3 mm with a length of 1.7 mm for $\mathtt{SL}_1$ and 2.15 mm for $\mathtt{SL}_2$, respectively.

Each PIN diode is activated through the incorporation of a dedicated biasing network $\mathtt{B}_1$ and $\mathtt{B}_2$ as shown in Fig. 1. Each biasing network is implemented as a high impedance line with a width of 0.07 mm that is terminated by two RF choke radial stubs $\mathtt{RF}_1$ and $\mathtt{RF}_2$. The total length for $\mathtt{B}_1$ and $\mathtt{B}_2$ is 3.7 mm and 8.6 mm, respectively. The DC ground for the two diodes is also implemented through a 0.07 mm biasing line $\mathtt{DC}_{\mathtt{gnd}}$ that is terminated by two identical RF choke radial stubs RF_3. For wideband operation, the three RF choke stubs have the corresponding radius and angle: $\mathtt{RF}_1$ (1.65 mm /60°), $\mathtt{RF}_2$ (1.5 mm /90°), and $\mathtt{RF}_3$(1.75 mm /60°).

The incorporation of these two PIN diodes along the corresponding biasing network enables the filter to achieve four reconfigurable bands. These reconfigurable bands are obtained based on the four states of the two PIN diodes (d_1-d_2: $\mathtt{off}_1$-$\mathtt{off}_2$, $\mathtt{on}_1$-$\mathtt{off}_2$, $\mathtt{off}_1$-$\mathtt{on}_2$, $\mathtt{on}_1$-$\mathtt{on}_2$). The integrated PIN diodes feature an insertion loss of 0.49 dB when activated. The simulated response ($|S_{11}|$ [dB]) of the proposed four-band reconfigurable filter is presented in Fig. 2(a). The first diode state $\mathtt{off}_1$-$\mathtt{off}_2$ enables the filter to cover the highest frequency band between 26.6 GHz and 29.5 GHz. A frequency shift is obtained upon the individual activation of the two integrated PIN diodes. Accordingly, for the PIN diodes' state $\mathtt{on}_1$-$\mathtt{off}_2$, the operating band changes to 25.4 – 27.25 GHz. The filter switches to 24.3 – 25.5 GHz for the state $\mathtt{off}_1$-$\mathtt{on}_2$. The lowest achieved band is obtained for the state $\mathtt{on}_1$-$\mathtt{on}_2$ where the filter operating bandwidth spans between 23.7 GHz and 24.7 GHz, respectively. The change in the filter's operating

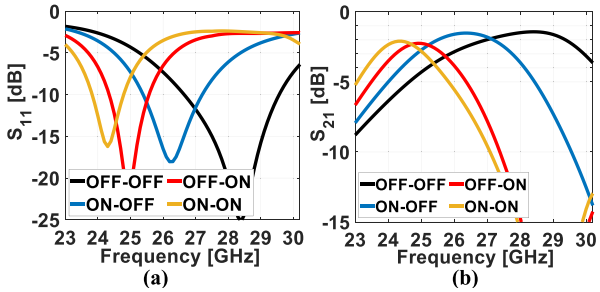

FIGURE 2. The simulated S-parameters for the reconfigurable filter based on the four different states of the two integrated PIN diodes: (a) $|S_{11}|$ [dB], (b) $|S_{21}|$ [dB].

bandwidth is obtained due to the change in the length of the open stubs. The filter's insertion loss, presented in Fig. 2(b), is less than 2 dB at the four frequency bands. The quality factor of the filter for the four states of the integrated PIN diodes are as follows: 5.12 ($\mathtt{off_1\text{-}off_2}$), 6.4 ($\mathtt{on_1\text{-}off_2}$), 8.2 ($\mathtt{off_1\text{-}on_2}$), and 8.3 ($\mathtt{on_1\text{-}on_2}$).

III. RECONFIGURABLE CIRCULARLY POLARIZED ANTENNA ARRAY

The design of a 16-element circularly polarized antenna array is proposed in this section. To obtain the required right hand circularly polarized radiation, the 16-element antenna array deploys two stages of sequential power divider networks. The frequency reconfiguration is then implemented through the appropriate integration of the modified ring resonator detailed in the previous section within the array's feeding network.

A. CIRCULARLY POLARIZED ANTENNA ARRAY DESIGN

The proposed antenna array, shown in Fig. 3(a), is composed of three parts. The first part is the 16-element array that can be decomposed into four identical subarrays.

The detailed dimensions of one of the four subarrays are depicted in Fig. 3(b). Each subarray employs four 3.3 mm x 3.4 mm truncated rectangular patches. Each radiating patch has a corner truncation of length 1.4 mm. The elements of a given subarray are orthogonally oriented with respect to each other and fed by a sequential power divider. Accordingly, four identical 1 x 4 sequentially rotated power dividers are incorporated to feed the four subarrays. Each sequential power divider has an input impedance of 50 Ω (point A in Fig. 3(b)) and four output ports with an impedance of 135Ω (points B1 to B4 in Fig. 3(b)). This output impedance is chosen to match the input impedance of the four truncated patches in each subarray. Thus, the objective of these four power dividers is to provide an equal power split between the four radiating patches of each subarray while ensuring an appropriate impedance transformation from 50Ω to 135Ω, respectively. The detailed dimensions of one of the four sequential power dividers are also included in Fig. 3(b).

The second part of the proposed array is the 0.5 mm thick RO3003 substrate with a full 34 mm x 32 mm ground plane. This substrate is stacked on top of a 0.13 mm thick RT 5870

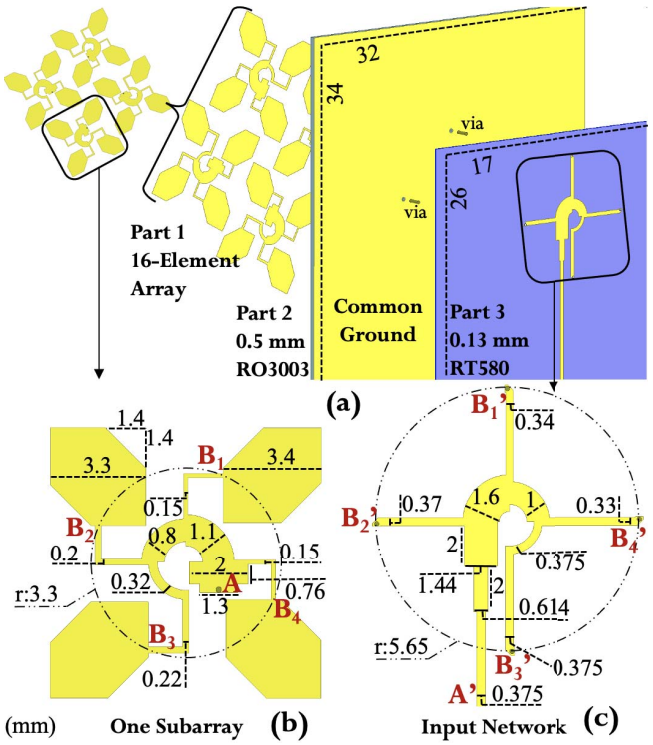

FIGURE 3. (a) The 16-element antenna array, (b) The structure of one of the four subarrays along with the first sequential power divider, (c) The second sequentially rotated power divider at the input of the array.

substrate ($\varepsilon_r = 2.33$ and $\tan\,\delta = 0.0012$), which constitutes the third layer. The two substrates are aligned through four vias that ensure the connection between the various layers. The third part incorporates a second sequential power divider that is printed on the bottom layer of a 0.13 mm thick RT5870 substrate. This part provides the connection between the RF input of the overall antenna array structure with the inputs of the power dividers in the four subarrays. Accordingly, as shown in Fig. 3(a), four vias are incorporated within the second part to provide the appropriate RF signal routing. The detailed dimensions of the power divider in the third part are shown in Fig. 3(c). The 50 Ω input port (point A' in Fig. 3(c)) of the power divider constitutes the input port of the overall array structure while its four output ports (points B1' to B4' in Fig. 3(c)) are designed with an impedance of 50 Ω to match the input port of the four subarrays.

A common ground is shared between the bottom layer of the second part and the top layer of the third part. The two dielectrics of the overall array structure are strategically selected since the thin RT5870 contributes to the size reduction of the various transmission lines and to a low loss feeding network, while the thick RO3003 contributes to attaining a larger operating bandwidth with an increased radiation efficiency. These design approaches result in multiple benefits such as distance reduction between the elements, SLL reduction, smaller antenna footprint, and circular polarization purity improvement.

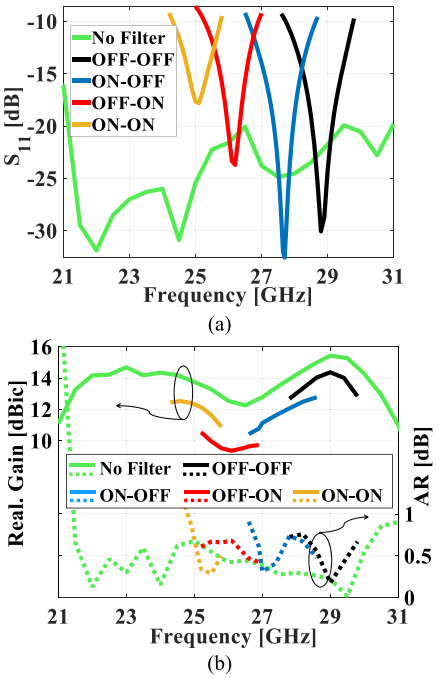

FIGURE 4. (a) The reflection coefficient for the 16-element array before and after the integration of the reconfigurable filter, (b) The realized gain [dBic] and axial ratio [dB] for the 16-element array before and after the integration of the reconfigurable filter.

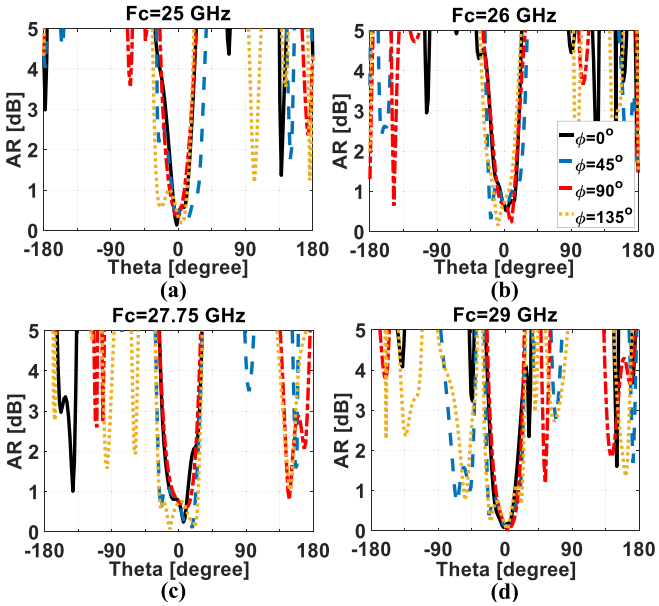

FIGURE 5. The axial ratio beamwidth for different Φ-planes at the four reconfigurable bands with center frequency (a) 25 GHz, (b) 26 GHz, (c) 27.75 GHz, (d) 29 GHz.

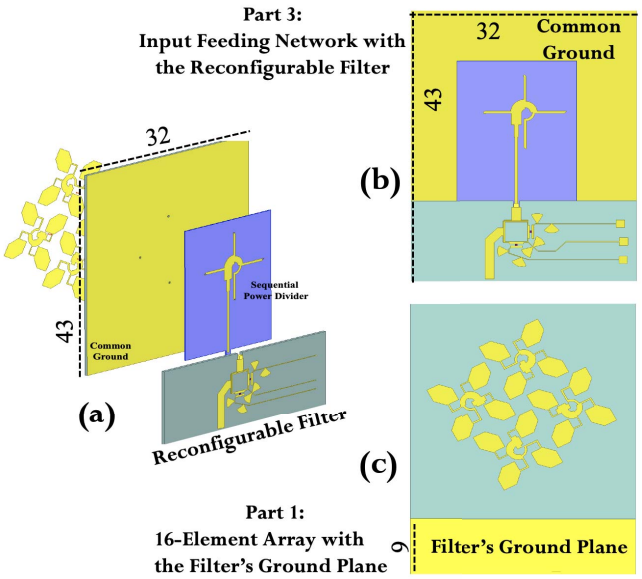

FIGURE 6. (a) The proposed frequency reconfigurable circularly polarized antenna array, (b) The layout for the third part of the array, and (c) for the first part.

The input reflection coefficient for the overall array structure is presented in Fig. 4(a). The proposed array is able to produce a good matching for the span of frequencies between 21 GHz and 31 GHz with a reflection coefficient less than −20 dB. The array's realized gain is more than 12 dBic with an axial ratio that remains less than 1 dB over the entire span of frequencies as presented in Fig. 4(b). In addition, Fig. 5 provides the axial ratio for different Φ-planes at the four reconfigurable bands with center frequencies of 25 GHz, 26 GHz, 27.75 GHz, and 29 GHz respectively. These results prove that over the entire array's operating bandwidth, a circularly polarized behavior with stable radiation characteristics is attained with a beamwidth of 30 degrees.

B. FREQUENCY RECONFIGURABLE ANTENNA ARRAY

The integration of the reconfigurable filter with the proposed antenna array is implemented in order to achieve a frequency reconfigurable antenna array with circular polarization radiation. Such frequency reconfigurability is essential to improve the selectivity of the proposed design and minimize the interference and noise that can be received by the array that operates originally over a wide bandwidth. The reconfigurable array topology is shown in Fig. 6(a). The reconfigurable filter is now integrated in the third part of the array and connects to the input port of the second sequential feeding network. Accordingly, the third part of the frequency reconfigurable antenna array is composed of the feeding network that is designed on a 0.13 mm thick RT5870 substrate cascaded by the reconfigurable filter that is designed on a 0.5 mm thick RO3003 substrate. The layout of the third part is shown in Fig. 6(b).

The ground plane of the filter with dimensions of 9 mm x 32 mm resides on the surface of the array along with the 16-element radiating patches as presented in Fig. 6(c). The connection between the filter's output port (width of 1.3 mm) to the input port of the feeding network (width of 0.375 mm) is achieved by adding a 0.6 mm x 0.715 mm x 0.6 mm matching section. This cubic metallic part provides the appropriate transition between the filter's output port and

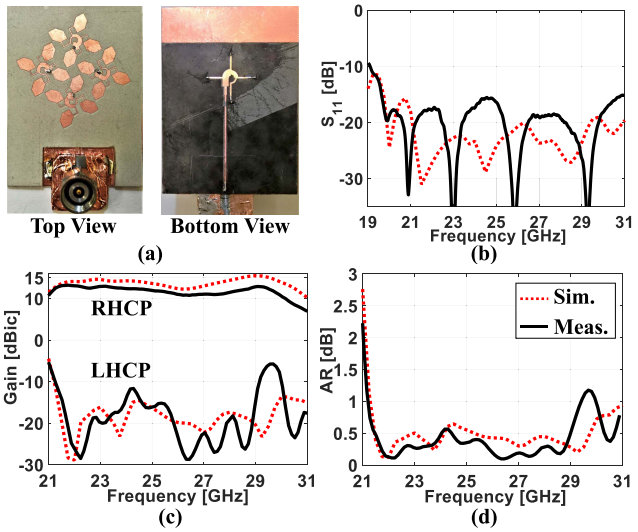

FIGURE 7. (a) The top and bottom views for the fabricated 16-Element antenna array, (b) The comparison between the simulated and measured results for the array's reflection coefficient, (c) RHCP and LHCP realized gain, and (d) axial ratio.

the array's input port. The second part, which is composed of the 0.5 mm thick RO3003 substrate with the four integrated vias, remains the same. A common ground plane in the bottom layer of the second part separates the array's radiating surface from the reconfigurable filter and the input feeding network. Such topology ensures better isolation between the guiding and radiating waves with a compact topology. The overall total dimensions of the array system are 43 mm x 32 mm.

The reflection coefficient plots for the reconfigurable antenna array structure are also included in Fig. 4(a) for the different states of the two integrated PIN diodes. The proposed array is now following the mode of operation of the reconfigurable filter by covering four distinct frequency bands. Fig. 4(b) also includes the realized gain and the axial ratio of the reconfigurable array. The integration of the filter hasn't impacted the circularly polarized behavior of the array since the dual sequentially rotated feeding networks are maintained within the overall structure. The integration of the reconfigurable filter has dropped the array's realized gain by almost 2 dBic for the different states of the PIN diodes. Such drop occurs as a result of the insertion loss of the filter that is produced mainly from the two integrated PIN diodes.

IV. MEASUREMENT RESULTS

A. FABRICATED CIRCULARLY POLARIZED ANTENNA ARRAY

The proposed circularly polarized antenna array is first fabricated as shown in Fig. 7(a) and tested to validate its performance. The comparison between the simulated and measured reflection coefficients is shown in Fig. 7(b). The fabricated prototype is able to preserve the wide operating bandwidth of the array, which covers a span of frequencies between 21 GHz and 31 GHz. The co- and cross-polarization

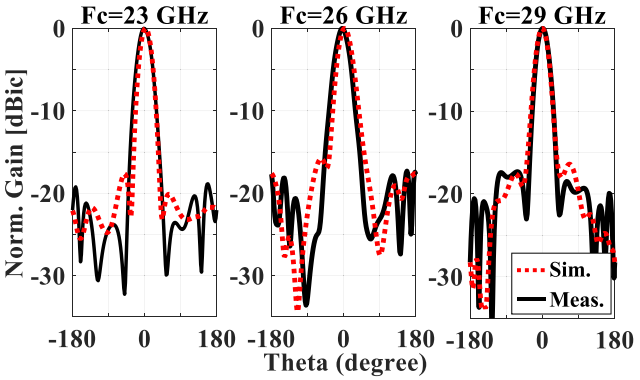

FIGURE 8. The simulated and measured radiation patterns for the proposed array at $\Phi = 90^{\circ}$ for three center frequencies 23 GHz, 26 GHz, and 29 GHz.

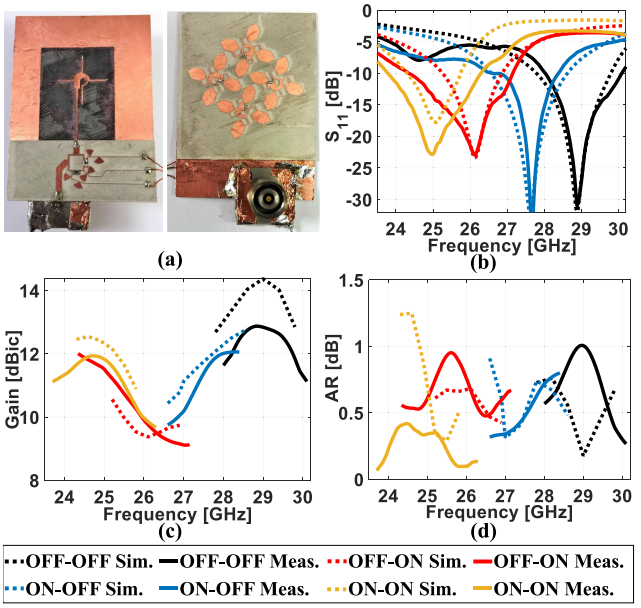

FIGURE 9. (a) The top and bottom views for the fabricated frequency reconfigurable antenna array, (b) The comparison between the simulated and measured results for the reconfigurable array's reflection coefficient, (c) co-polarized realized gain, and (d) axial ratio.

realized gain plots are shown in Fig. 7(c), where the measured RHCP gain is greater than 10 dBic. A difference that exceeds 20 dB is obtained between the two polarization schemes. This proves the excellent polarization discrimination of the designed array. It is noticed that a little difference is obtained between the measured and simulated gain values. This difference is mainly due to the losses introduced by the copper rods used as vias to connect the various parts of the array. The measured axial ratio presented in Fig. 7(d) also agrees with the simulated one, confirming the achieved pure circular polarization. The measured radiation patterns at 23 GHz, 26 GHz, and 29 GHz in $\Phi = 90^{o}$ plane are shown in Fig. 8. The three measured patterns demonstrate good agreement with the simulated ones where side lobe levels of -19 dB, -18 dB, and -17.5 dB respectively are obtained for the three operating frequencies.

TABLE 1. Comparisons with other millimeter-wave circular polarized arrays.

Ref.	NE	Fc / FBW	Gain Peak dBic / 3dB FBW	FBW of AR<1dB	SLL	FOM	Antenna Topology	Feeding Method	Power Divider	Element Pol.	Element Band	System Pol.
[15]	64	37.5/35.4	23.5/32.2	7.36	11	2.51	Stack	Aperture	Parallel	Circular	Broad	Circular
[16]	64	29 / 13.8	N/A/3.07	2.8	11	10.03	One Layer	Direct TL	Sequential	Circular	Narrow	Circular
[17]	4	29.7/15.4	13.59/20.2	0	22	0	One Layer	Direct TL	Sequential	Circular	Narrow	Circular
[18]	4	45.5/19.8	10.5/14.7	7.7	10	5.24	Stack	Aperture	Sequential	Linear	Broad	Circular
[19]	16	59.9/22	15.98/9.5	0	10	0	One Layer	Direct TL	Sequential	Linear	Broad	Circular
[20]	64	31/22	23/15.43	11.45	13	9.65	Stack	Aperture	Sequential	Circular	Broad	Circular
This Work	**16**	**26/38.5**	**13/35.3**	**35.8**	**17.5***	**17.75**	**Stack**	**Vias**	**Sequential**	**Elliptical**	**Dual**	**Circular**

NE: Number of Elements.
AR: Axial Ratio calculated from the refer. graphs.
Fc: Center Frequency [GHz].
FBW: Fractional Bandwidth [%].
SLL: Side Lobe Level [-dB] @Φ=90°
*: SLL for the frequency range 21.5-30GHz.
FOM: Figure of Merit [dB]

TABLE 2. Comparisons with other frequency reconfigurable arrays at K/KA-band.

Ref.	Element Type	Fc	Recon. Bands	Freq. Range	Active Component	Number of Components	Voltage [V]	Peak Gain	System Pol.
[21]	Aperture	28	2	27.65-29.1	Pin Diode	2	3	6.4	Linear
[22]	Microstrip Patch	28	Cont.	26.9-30.8	Liquid Crystal	N/A	20	6.5	Linear
This Work	**Microstrip Patch**	**26**	**4**	**23.75-30.1**	**Pin Diode**	**2**	**3**	**13**	**Circular**

A comparative analysis with other existing millimeter-wave circularly polarized antenna arrays available in the literature is presented in Table 1. This table includes a Figure of Merit (FoM) to highlight the superior radiation characteristics of the proposed antenna array.

$$\text{FOM(dB)} = \frac{\text{FBW of AR}}{\text{FBW of CP Gain}} \times |\text{SLL}| \qquad (1)$$

The FoM, defined in Eq. (1), includes several design specifications. The first design parameter is the 3 dB fractional bandwidth (FBW) of circularly polarized gain with reference to the peak gain. This factor considers the useful operating bandwidth while assuming the circular polarization behavior of the antenna. The second parameter is the FBW when the axial ratio (AR) is less than 1 dB. This ensures circular polarization performance with very low AR. The last factor is the absolute sidelobe level of the radiation pattern, which ensures interference reduction in the operating bandwidth. These factors constitute the main parameters of the proposed FOM, where the greatest value is interpreted as the most efficient model according to the set requirements. The presented structure herein features the highest FOM (i.e., 17.75 dB) in comparison to the other referenced work in Table 1. Such level of FOM emphasizes the improved radiation behavior of the designed 16-element antenna array structure presented herein.

B. FABRICATED FREQUENCY RECONFIGURABLE ARRAY

The proposed frequency reconfigurable array is fabricated next to assess its radiation characteristics and validate that the integration of the reconfigurable filter does not impact the circularly polarized behavior of the array. The corresponding fabricated prototype is presented in Fig. 9(a) where the reconfigurable filter is shown on the top view of the structure. The reflection coefficient response is shown in Fig. 9(b) with the measured resonant frequencies analogously matching the simulated ones. The first state ($\texttt{off}_1\texttt{-off}_2$) of the antenna operates at 28 – 30.1 GHz, the second state ($\texttt{on}_1\texttt{-off}_2$) operates at 26.7 – 28.4 GHz, the third state ($\texttt{off}_1\texttt{-on}_2$) covers the band 24.4 – 27.1 GH, and finally, the last state ($\texttt{on}_1\texttt{-on}_2$) covers the band 23.75 – 26.3 GHz. Thus, the antenna array can cover an overall frequency range of 23.75 – 30.1 GHz for the four different states of the two integrated PIN diodes. Next, Fig. 9(c) depicts the simulated and measured RHCP realized gain performance of the reconfigurable array at the four different bands. The measured realized gain at the center resonant frequency for each reconfigurable state is 12 dBic ($\texttt{on}_1\texttt{-on}_2$), 10 dBic ($\texttt{off}_1\texttt{-on}_2$), 12 dBic ($\texttt{on}_1\texttt{-off}_2$), and 13 dBic ($\texttt{off}_1\texttt{-off}_2$) respectively. The measured results are in good accordance with the simulated ones, while the 1.2 dB variation at the higher frequencies ($\texttt{off}_1\texttt{-off}_2$ state) is mainly due to the various fabrication tolerances whose effect is more pronounced with an increase in the operating frequency. The axial ratio of the reconfigurable antenna array system is illustrated in Fig. 9(d), which is less than 1 dB for all the operational bands. Fig. 10 shows the normalized radiation pattern for the reconfigurable center frequencies 25 GHz, 26 GHz, 27.75 GHz, and 29 GHz in the $\Phi = 90°$ plane. The four measured patterns show good agreement with the simulated ones, with a sidelobe level less than -15 dB for all the four different states.

Table 2 compares the presented frequency reconfigurable array with other existing reconfigurable antennas operating

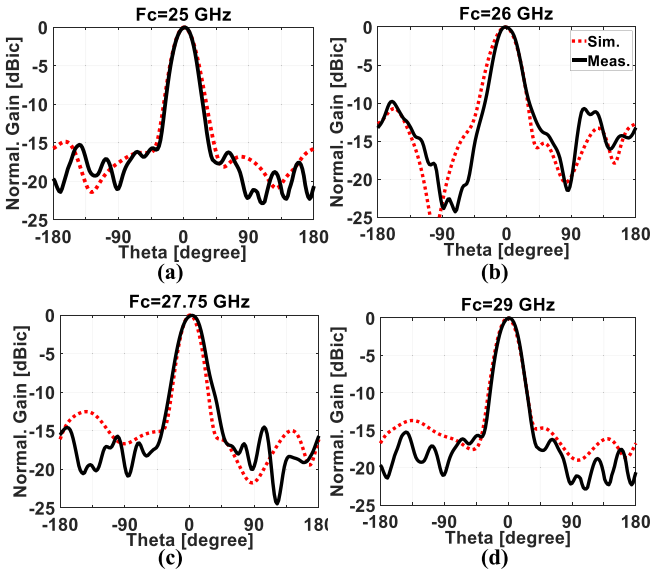

FIGURE 10. The simulated and measured radiation patterns of the reconfigurable 16-Element array at $\Phi = 90°$ for the (a) on-on state – 25 GHz, (b) on-off state – 26 GHz, (c)off-on state – 27.75 GHz, and (d) off-off state – 29 GHz.

at K/Ka bands in the literature. The presented work herein features unique characteristics in achieving circularly polarized radiation over four distinct bands with a maximum gain of almost 13 dBic.

V. CONCLUSION

This work proposes a millimeter-wave frequency reconfigurable circularly polarized antenna array. The proposed structure consists of a frequency reconfigurable modified ring resonator filter integrated within the feeding network of a 16-element antenna array. The frequency reconfiguration is achieved over four distinct bands through the activation of two integrated PIN diodes, thus covering the span of frequencies between 23.75 GHz and 30.1 GHz. The presented antenna array achieves distinguished radiating characteristics, such as an almost pure polarization (AR$<$1 dB) in a FBW of 35.8%, sidelobe level less than -17.5 dB, and a gain greater than 13 dBic. A comparison with related work and the 17.75 dB figure of merit index, displays the superior performance of the proposed antenna array.

REFERENCES

[1] L. Huitema, Y. Dia, M. Thevenot, S. Bila, A. Perigaud, and C. Delaveaud, "Miniaturization of a filter-antenna device by co-design," *IEEE Open J. Antennas Propag.*, vol. 2, pp. 498–505, 2021.

[2] L. Santamaria, F. Ferrero, R. Staraj, and L. Lizzi, "Electronically pattern reconfigurable antenna for IoT applications," *IEEE Open J. Antennas Propag.*, vol. 2, pp. 546–554, 2021.

[3] M. Patriotis, F. N. Ayoub, C. G. Christodoulou, and M. T. Chryssomallis, "A reconfigurable K/Ka band filtenna using a double arm ring resonator," in *Proc. IEEE Int. Symp. Antennas Propag. USNC-URSI Radio Sci. Meeting*, 2019, pp. 1479–1480.

[4] Y. Tawk, J. Costantine, and C. G. Christodoulou, "Reconfiguring the frequency and directive behavior of a printed V–shaped structure," *IEEE Trans. Antennas Propag.*, vol. 65, no. 5, pp. 2655–2660, May 2017.

[5] H. A. Atallah, A. B. Abdel-Rahman, K. Yoshitomi, and R. K. Pokharel, "Compact frequency reconfigurable filtennas using varactor loaded T-shaped and H-shaped resonators for cognitive radio applications," *IET Microw. Antennas Propag.*, vol. 10, no. 9, pp. 991–1001, 2016.

[6] Y. Tawk, J. Costantine, and C. G. Christodoulou, "Reconfigurable filtennas and MIMO in cognitive radio applications," *IEEE Trans. Antennas Propag.*, vol. 62, no. 3, pp. 1074–1083, Mar. 2014.

[7] T. Cheng and K.-W. Tam, "A wideband bandpass filter with reconfigurable bandwidth based on cross-shaped resonator," *IEEE Microw. Compon. Lett.*, vol. 27, no. 10, pp. 909–911, Oct. 2017.

[8] A. Miller and J.-S. Hong, "Wideband bandpass filter with reconfigurable bandwidth," *IEEE Microw. Compon. Lett.*, vol. 20, no. 1, pp. 28–30, Jan. 2010.

[9] H.-J. Tsai, N.-W. Chen, and S.-K. Jeng, "Center frequency and bandwidth controllable microstrip bandpass filter design using loop-shaped dual-mode resonator," *IEEE Trans. Microw. Theory Techn.*, vol. 61, no. 10, pp. 3590–3600, Oct. 2013.

[10] K. Chang and L. Hsieh, *Microwave Ring Circuits and Related Structures*, 2nd ed. Hoboken, NJ, USA: Wiley, 2004.

[11] L.-H. Hsieh, "Analysis, modeling and simulation of ring resonators and their applications to filters and oscillators," Ph.D. dissertation, Dept. Elect. Eng., Texas A&M Univ., College Station, TX, USA, 2004.

[12] C.-C. Yu and K. Chang, "Transmission-line analysis of a capacitively coupled microstrip-ring resonator," *IEEE Trans. Microw. Theory Techn.*, vol. 45, no. 11, pp. 2018–2024, Nov. 1997.

[13] S. Sun and L. Zhu, "Wideband microstrip ring resonator bandpass filters under multiple resonances," *IEEE Trans. Microw. Theory Techn.*, vol. 55, no. 10, pp. 2176–2182, Oct. 2007.

[14] C. H. Kim and K. Chang, "Ring resonator bandpass filter with switchable bandwidth using stepped-impedance stubs," *IEEE Trans. Microw. Theory Techn.*, vol. 58, no. 12, pp. 3936–3944, Dec. 2010.

[15] Q. Wu, J. Hirokawa, J. Yin, C. Yu, H. Wang, and W. Hong, "Millimeter-wave planar broadband circularly polarized antenna array using stacked curl elements," *IEEE Trans. Antennas Propag.*, vol. 65, no. 12, pp. 7052–7062, Dec. 2017.

[16] A. Chen, Y. Zhang, Z. Chen, and C. Yang, "Development of a Ka-band wideband circularly polarized 64-element microstrip antenna array with double application of the sequential rotation feeding technique," *IEEE Antennas Wireless Propag. Lett.*, vol. 10, pp. 1270–1273, 2011.

[17] A. Chen, Y. Zhang, Z. Chen, and S. Cao, "A Ka-band high-gain circularly polarized microstrip antenna array," *IEEE Antennas Wireless Propag. Lett.*, vol. 9, pp. 1115–1118, 2010.

[18] Y. Zhang, W. Hong, and R. Mittra, "45 GHz wideband circularly polarized planar antenna array using inclined slots in modified short-circuited SIW," *IEEE Trans. Antennas Propag.*, vol. 67, no. 3, pp. 1669–1680, Mar. 2019.

[19] B. Lee and Y. Yoon, "Low-profile, low-cost, broadband millimeter wave antenna array for high-data-rate WPAN systems," *IEEE Antennas Wireless Propag. Lett.*, vol. 16, pp. 1957–1960, 2017.

[20] M. Akbari, A. Farahbakhsh, and A.-R. Sebak, "Ridge gap waveguide multilevel sequential feeding network for high-gain circularly polarized array antenna," *IEEE Trans. Antennas Propag.*, vol. 67, no. 1, pp. 251–259, Jan. 2019.

[21] J. Choi *et al.*, "Frequency-adjustable planar folded slot antenna using fully integrated multithrow function for 5G mobile devices at millimeter-wave spectrum," *IEEE Trans. Microw. Theory Techn.*, vol. 68, no. 5, pp. 1872–1881, May 2020.

[22] J. Kim and J. Oh, "Liquid-crystal-embedded aperture-coupled microstrip antenna for 5G applications," *IEEE Antennas Wireless Propag. Lett.*, vol. 19, no. 11, pp. 1958–1962, Nov. 2020.

MARIOS PATRIOTIS (Student Member, IEEE) received the Diploma degree in electrical and computer engineering from the Democritus University of Thrace, Xanthi, Greece, in 2016, and the M.S. degree from The University of New Mexico, Albuquerque, NM, USA, in 2019, where he is currently pursuing the Ph.D. degree with Antennas & RF Lab. His research interests include reconfigurable microwave matching networks and diversity antennas for millimeter wave systems.

FIRAS N. AYOUB received the B.E. degree from the American University of Beirut, Beirut, Lebanon, in 2011, and the M.S. and Ph.D. degrees from the University of New Mexico, Albuquerque, NM, USA, in 2013 and 2018, where he is currently an Assistant Research Professor with Electrical and Computer Engineering Department and an RF Engineer with TransCore. He is the Co-Inventor on two U.S. patents, and he has authored and coauthored more than 30 IEEE journals and conference papers. His research interests include mm-wave antennas, reconfigurable antenna arrays using nematic liquid crystal and reconfigurable RF components and RFID.

YOUSSEF TAWK (Senior Member, IEEE) received the Bachelor of Engineering degree (with Highest Distinction) from Notre Dame University Louaize in Fall 2006, and the master's degree in engineering degree from the American University of Beirut, Lebanon, in 2007, and the Ph.D. degree from the University of New Mexico, Albuquerque, NM, USA, in 2011. He is an Assistant Professor with Electrical and Computer Engineering Department, American University of Beirut. He served as the Valedictorian of his graduating class with Notre Dame University Louaize. He has coauthored of two books and one book chapter, and a Co-Inventor on seven U.S. patents. His research interests include reconfigurable RF systems for microwave and mm-wave applications, cognitive radio, optically controlled RF components, phased arrays, and phase shifters based on smart RF materials. Throughout his education and career, he has received many awards and honors, such as the 2018 and 2014 Science and Technology Innovation Award for his patents on reconfigurable microwave filters and optically controlled antenna systems in addition to the 2011 IEEE Albuquerque Chapter Outstanding Graduate Award. He has more than 150 IEEE journals and conference papers many of which received finalist positions and honorable mentions in several paper contests.

JOSEPH COSTANTINE (Senior Member, IEEE) received the bachelor's degree from the second branch of the Faculty of Engineering, Lebanese University, the master's (M.E.) degree from the American University of Beirut, and the Doctoral degree from the University of New Mexico in 2009. He is an Associate Professor with the Electrical and Computer Engineering Department, American University of Beirut and a World Economic Forum Young Scientist. He has 11 Provisional and Full U.S. patents. He has published so far two books, one book chapter and more than 150 Journal and conference papers. His research interests reside in reconfigurable antennas, cognitive radio, RF energy harvesting systems, antennas and rectennas for IoT devices, RF systems for biomedical devices, wireless characterization of dielectric material, and deployable antennas for small satellites. He received many awards and honors throughout his career, including the 2008 IEEE Albuquerque Chapter Outstanding Graduate Award, the three year (2011–2013) Air Force Summer Faculty Fellowship with Kirtland's space vehicles directorate in NM, USA, the 2017 First Prize at the Idea-Thon of International Healthcare Industry Forum, the 2019 Excellence in Teaching Award from American University of Beirut, the 2018 and 2020 STC Science and Technology Innovation Awards, and the 2020 Distinguished Young Alumni Award from the School of Engineering at the University of New Mexico. He has been an Associate Editor for the IEEE ANTENNAS AND WIRELESS PROPAGATION LETTERS since July 2018.

CHRISTOS G. CHRISTODOULOU (Life Fellow, IEEE) received the Ph.D. degree in electrical engineering from North Carolina State University in 1985.

He is currently the Dean of the School of Engineering and Computing, University of New Mexico. He has published over 570 papers in journals and conferences, written 17 book chapters, coauthored nine books, and has several patents. He is a recipient of the 2010 IEEE John Krauss Antenna Award for his work on reconfigurable fractal antennas using MEMS switches and has been inducted in the Alumni Hall of Fame for the Electrical and Computer Engineering Department, North Carolina State University, in 2016. He served as an Associate Editor for the IEEE TRANSACTIONS ON ANTENNAS AND PROPAGATION for six years. He served as a Co-Editor for a special issue on "Reconfigurable Systems" in the IEEE Proceedings (March 2015), a Co-Editor of the IEEE ANTENNAS AND PROPAGATION Special issue on "Synthesis and Optimization Techniques in Electromagnetics and Antenna System Design" (March 2007), and for the Special issue on *Antenna Systems and Propagation for Cognitive Radio* in 2014. Since 2013, he has been serving as the Series Editor for Artech House Publishing company for the area of Antennas and Propagation. He was appointed as an IEEE AP-S Distinguished Lecturer from 2007 to 2010. He is a member of Commission B of the U.S. National Committee for URSI, and a Distinguished Professor with UNM.